Spin–orbit torques and magnetization switching in W/Co_2FeAl/MgO structures

2016 J. Phys. D: Appl. Phys. 49 365003

(http://iopscience.iop.org/0022-3727/49/36/365003)

IOP Publishing Journal of Physics D: Applied Physics
J. Phys. D: Appl. Phys. **49** (2016) 365003 (7pp) doi:10.1088/0022-3727/49/36/365003

Spin–orbit torques and magnetization switching in W/Co_2FeAl/MgO structures

M S Gabor[1], T Petrisor Jr[1], R B Mos[1], A Mesaros[1], M Nasui[1], M Belmeguenai[2], F Zighem[2] and C Tiusan[1,3]

[1] Center for Superconductivity, Spintronics and Surface Science, Physics and Chemistry Department, Technical University of Cluj-Napoca, Str. Memorandumului, 400114 Cluj-Napoca, Romania
[2] LSPM (CNRS-UPR 3407), Université Paris 13, Sorbonne Paris Cité, 99 avenue Jean-Baptiste Clément, 93430 Villetaneuse, France
[3] Institut Jean Lamour, CNRS, Université de Lorraine, 54506 Vandoeuvre, France

E-mail: mihai.gabor@phys.utcluj.ro

Received 3 April 2016, revised 24 May 2016
Accepted for publication 27 May 2016
Published 17 August 2016

Abstract

Magnetization switching by current induced spin–orbit torques (SOTs) in heavy metal/ferromagnetic metal/oxide structures is of great research interest due to its potential applications in the field of low power consumption spintronic devices. Here, we study the Slonczewski-like and the field-like SOT effective fields in β-W/Co_2FeAl/MgO structures showing perpendicular magnetic anisotropy (PMA). We characterize the SOT effective fields using harmonic Hall voltage measurements and we point out the essential role of the planar Hall effect corrections. We estimate that for bulk β-W an effective spin Hall angle as large as 0.3 ± 0.03 and a spin diffusion length of 2.2 ± 0.3 nm. Moreover, we demonstrate SOT-induced magnetization switching for charge current densities of the order of 10^6 A cm^{-2}.

Keywords: Heusler alloys, spin orbit torques, perpendicular magnetic anisotropy

(Some figures may appear in colour only in the online journal)

Introduction

Current-induced spin–orbit torques (SOTs) in ultrathin ferromagnetic layers interfaced with a heavy metal and an oxide have recently attracted considerable research interest for the development of low power consumption spintronic devices. To date, SOTs have been used to realize current-induced magnetization switching [1–4], fast domain-wall motion [5–10] and high frequency magnetization oscillation [11–13]. Although still under debate, in this type of system, SOTs have been attributed to the spin Hall effect (SHE) within the heavy metal [2, 3, 14] and/or to the Rashba effect arising from the lack of structural inversion symmetry within the heavy metal/ferromagnet/oxide structure [6, 15–17]. Independently from their origin, the SOTs are equivalent with two types of effective fields, such as the Slonczewski-like (H^{SL}) and the field-like (H^{FL}) effective field [2, 6, 16]. The field-like effective field has a direction given by the unit vector $\hat{y}$ which is in-plane and transverse to the electrical current, while the Slonczewski-like effective field is oriented along the $\hat{y} \times \hat{m}$ direction ($\hat{m}$ is a unit vector parallel with the magnetization vector), and it is responsible for the magnetization switching. In the SHE picture, the SOTs are due to angular momentum transfer from the spin-current, which is generated within the heavy metal via SHE, to the magnetization of the ferromagnetic layer. Therefore, the SOT's efficiency is directly connected to the ratio of the spin-current generated per unit of the in-plane charge current flowing through the heavy metal layer and it is parametrized by the spin Hall angle (θ_{SH}). Among the transition heavy metal materials, tungsten, in metastable β phase, is considered to have the largest spin Hall angle (around 0.3) [14].

In this paper, we investigate the current induced Slonczewski-like (H^{SL}) and the field-like (H^{FL}) effective fields in perpendicularly magnetized β-W/Co_2FeAl/MgO structures. We demonstrate the attainment of perpendicular magnetic anisotropy (PMA), a key aspect for scalability of spintronic devices, without the need of magnetic annealing, which could be detrimental for the stabilization of the β-W metastable phase [14]. The ferromagnetic layer we have

chosen is a Co_2FeAl full-Heusler alloy, which is an attractive material for spintronic applications, since it was shown to provide large spin polarization [18] and to possess a low Gilbert damping [19], which are essential attributes for efficient switching, domain wall motion and magnetization oscillations generation. Using harmonic Hall measurements, we evaluate the SOT effective fields and point out the important role of the planar Hall effect (PHE) corrections. Therefore, we show that both effective fields show relatively large values and induce magnetization switching for charge current densities of the order of 10^6 A cm^{-2}.

Experiment

The Si/SiO_2/W(t nm)/CFA(0.8 nm)/MgO(1.0 nm)/Ta(2 nm) structures, with $t = 3.5$, 4.5, 5.5, 6.5 and 7.5 nm, were elaborated using a magnetron sputtering system having a base pressure lower than 2×10^{-8} Torr. The metallic films were deposited at room temperature (RT) by DC sputtering under an Ar pressure of 1 mTorr. The W films were deposited at a relatively low deposition rate of 1.6 nm min^{-1}, in order to facilitate the formation of the β phase. For the growth of the CFA layer, a 2 in Co_2FeAl stoichiometric target was used. The MgO film was grown at RT by rf sputtering from a MgO polycrystalline target in an Ar pressure of 10 mTorr. Finally, the stack was capped with a 2 nm thick Ta film in order to protect the structure from oxidation due to air exposure. After deposition, the samples were patterned for transport measurements, using UV lithography and Ar ion milling in the form of standard Hall bars with longitudinal and lateral dimensions of 100 μm and 30 μm, respectively (figure 2(a)). A second lithographic step was employed in order to allow the deposition of Ta (5 nm)/Cu(100 nm)/Ta(5 nm) contact pads. The magneto-transport measurements were performed using standard DC and AC lock-in techniques. The crystal structure of the films was investigated using a four circle diffractometer, while the saturation magnetization was determined using a vibrating sample magnetometer.

Results and discussions

Weconfirmed the formation of the β-W phase by performing x-ray diffraction measurements in grazing incidence geometry (GIXRD). Figure 1 shows the diffraction pattern for the W(5.5 nm)/CFA(0.8 nm)/MgO(1.0 nm) sample, which indicated the presence of β-W (2 0 0), (2 1 0) and (2 1 1) reflections. In the limit of resolution of the XRD experiments, no α-W phase reflections were observed. Figure 2(b) shows the W layer thickness dependence of the conductance of the patterned elements. Assuming the top capping Ta layer is fully oxidized and there is no current flow through it, the slope of the linear fit of the data provides the W layer resistivity, which was found to be around 160 $\mu\Omega$ cm. This is consistent with the attainment of the β-W phase [14], which is in agreement with the XRD measurements.

Regardless of the W layer thickness, the as-grown CFA films exhibit PMA, which is confirmed by the square shape

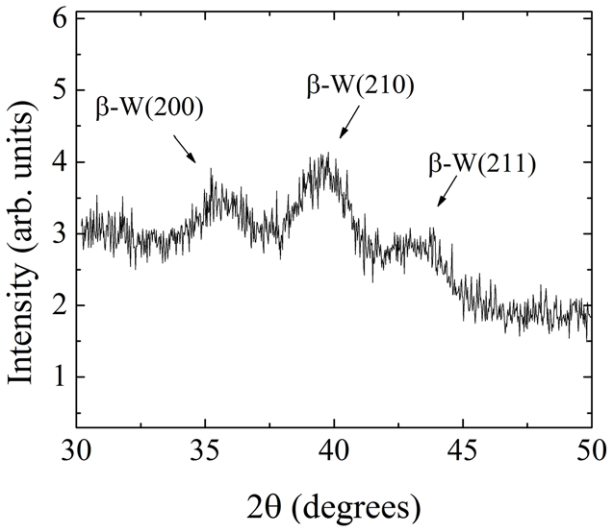

Figure 1. X-ray diffraction pattern measured in grazing incidence geometry (GIXRD) for the W(5.5 nm)/CFA(0.8 nm)/MgO(1.0 nm)/Ta(2 nm) structure. The positions of the β-W (2 0 0), (2 1 0) and (2 1 1) reflections are indicated.

of the Hall resistance versus perpendicular-to-plane magnetic field loop, as shown in figure 2(c) for the W(5.5 nm)/CFA(0.8 nm)/MgO(1.0 nm) structure. Furthermore, an in-plane saturation field of about $H_k = 3$ kOe and a saturation magnetization (M_s) of around 830 ± 100 emu cm^{-3}, were measured.

The SOT fields were quantified using harmonic Hall voltage measurements [20, 21]. The measurements geometry is depicted in figure 3(a). A 593 Hz sinusoidal current (along $\hat{x}$ was passed through the micro-strip and the first (V^{ω}) and second harmonic ($V^{2\omega}$) transverse voltages (along $\hat{y}$) were measured using the lock-in amplifier technique. The magneto-transport experiments were performed in two different configurations: the longitudinal one, with the external magnetic field applied along the x-axis (H_L); and the transverse one, with the external magnetic field applied along the y-axis (H_T). In order to avoid magnetization switching and domain wall formation, an out-of-plane magnetic field of about 40 Oe was applied during measurements. The two measuring configurations allow quantifying the longitudinal and the transverse effective fields (H^{SL} and H^{FL}) induced by the Slonczewski-like and by the field-like spin orbit torques using the equations [20]:

$$H^{SL} = -2\frac{\partial V^{2\omega}}{\partial H_L}\Big/\frac{\partial^2 V^{\omega}}{\partial H_L^2}$$
$$H^{FL} = -2\frac{\partial V^{2\omega}}{\partial H_T}\Big/\frac{\partial^2 V^{\omega}}{\partial H_T^2}. \quad (1)$$

Figures 3(b)–(e) show the first (V^{ω}) and the second harmonic ($V^{2\omega}$) voltages versus longitudinal (H_L) and transverse (H_T) swept external magnetic fields measured for the W(5.5 nm)/CFA(0.8 nm)/MgO(1.0 nm) sample, at a current density through the micro-stripe of $j = 1.06 \times 10^6$ A cm^{-2}. As expected, V^{ω} shows a parabolic dependence versus $H_{L(T)}$ due to the magnetization tilting from the vertical axis with the application of the external magnetic field. $V^{2\omega}$ shows a linear

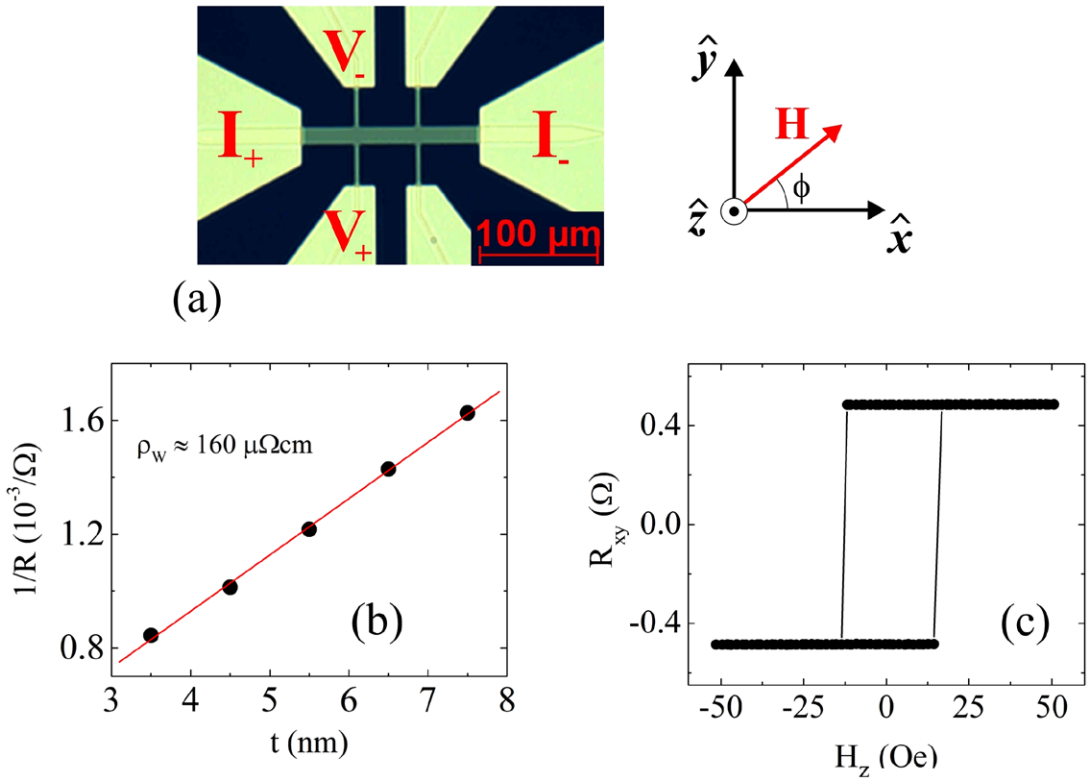

Figure 2. (a) Optical microscopy image of the Hall patterned device and the dc experiment configuration. (b) Electrical conductance of the patterned devices versus the thickness of the W layer. The red line is a linear fit of the data. (c) Anomalous Hall measurements for the W(5.5 nm)/CFA(0.8 nm)/MgO(1.0 nm) structure, showing the presence of the perpendicular magnetic anisotropy.

dependence versus $H_{L(T)}$ and, furthermore, the slope changes sign, when the magnetization changes sign, in the case of the transverse swept field. In order to determine the Slonczewski-like (H^{SL}) and the field-like (H^{FL}) induced effective fields using the equation (1), the first and second harmonic signals were fitted using quadratic and linear functions. The H^{SL} and H^{FL} SOT induced effective fields were determined using equation (1), and are plotted with respect to the charge current density (j) in figures 4(a) and (b). The effective fields vary linearly with j, suggesting that Joule heating and other non-linear effects are negligible in this current density range. The H^{SL} was found to be about −30.8 Oe (28.4 Oe) for 'up' ('down') magnetized configuration at a current density of $j = 10^6$ A cm^{-2}. Similarly, H^{FL} was found to be about 52.6 Oe (50.4 Oe) for 'up' ('down') magnetized configuration at a current density of $j = 10^6$ A cm^{-2}. However, this type of analysis has to be furthermore refined. It was pointed out that since the measured transverse voltage contains, in general, contributions from both the anomalous Hall effect (AHE) and PHE, a correction must be introduced in equation (1) when the two contributions are comparable [21–23] and the corrected effective fields will be given by:

$$H_C^{SL(FL)} = \frac{H_{SL(FL)} \pm 2\xi H_{FL(SL)}}{1 - 4\xi^2}, \qquad (2)$$

where the ± sign refers to the refers to the 'up' and 'down' magnetized configurations, while ξ is the ratio between the planar (ΔR_{PHE}) and anomalous (ΔR_{AHE}) Hall resistances. Since the measured transverse voltage contains contributions from both the anomalous and the planar effect, the corresponding resistance can be written as:

$$R_{xy} = \Delta R_{AHE} \cos\theta + \Delta R_{PHE} \sin^2\theta \sin 2\phi, \qquad (3)$$

where the θ and ϕ angles are defined in figure 3(a). In order to extract the AHE component, we have performed transverse resistance measurements with the magnetic field applied perpendicular to the sample plane (see the geometry depicted in figure 2(a) and the data in figure 2(c)) and we have determined the AHE contribution as: $\Delta R_{AHE} = [R_{xy}(\theta = 0) - R_{xy}(\theta = \pi)]/2$. The PHE measurements were performed by applying a 8.5 kOe in-plane magnetic field (larger than the in-plane saturation field) and rotating the sample about the vertical axis. In order to extract the PHE component, the data were fitted with equation (3), for $\theta = \pi/2$, as shown in figure 5(a) for the W(5.5 nm)/CFA(0.8 nm)/MgO(1.0 nm) sample. Figure 5(b) shows the W layer thickness dependence of ΔR_{PHE}, ΔR_{AHE} and of the ξ ratio. Both ΔR_{PHE} and ΔR_{AHE} decrease with increasing the W layer thickness, as expected due to the increased current shunting through the W layer. However, the decreasing rate is different for the two components. Moreover, ξ shows exceptionally large values which increase with increasing the W layer thickness. These facts suggest that there is an additional mechanism, besides the current shunting that is responsible for the ΔR_{PHE} and ΔR_{AHE} dependence on the W layer thickness. Large values of ξ were also observed in similar samples comprising W seed layers and were attributed to the giant spin Hall magnetoresistance (SMR) [24–26] due to the W layer, which strongly alters both the diagonal and off-diagonal elements of the resistivity tensor [27–29].

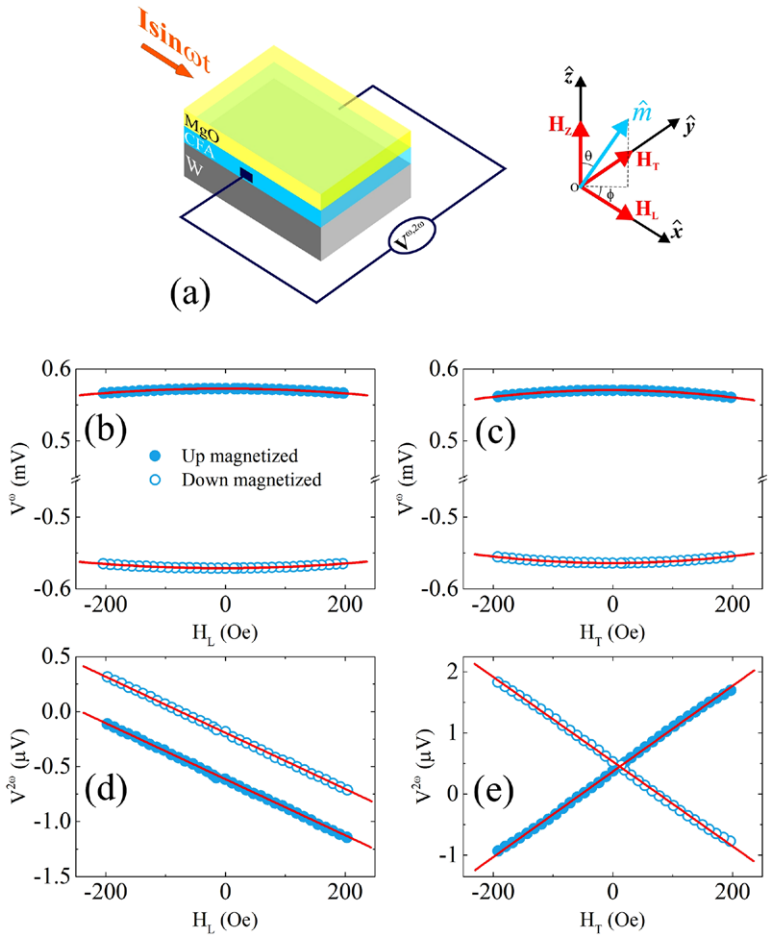

Figure 3. (a) Schematic illustration of the W/CFA/MgO structure and harmonic Hall magneto-transport measurement geometry. (b), (c) First (V^{ω}) and (d), (e) second harmonic ($V^{2\omega}$) voltages versus longitudinal and transverse swept magnetic fields. Filled and empty symbols correspond to 'up' and 'down' magnetized states, respectively. The red lines stand for quadratic and linear fits.

However, since the transverse resistance change due to the SMR shares a similar magnetization dependence as the PHE [29], its effects on the transverse resistance is just to add a constant value to the prefactor of the second term in equation (3). This ensures that the correction strategy of the spin orbit induced effective fields, which is employed in order to obtain equation (2), remains valid even in the presence of a giant SMR effect.

Figures 4(c) and (d) show the Slonczewski-like (H_C^{SL}) and the field-like (H_C^{FL}) SOT induced effective fields corrected using equation (2). It is important to point out that due to the relative large values of ξ both H_C^{SL} and H_C^{FL} show a significant decrease in the absolute value from -30.8 Oe (28.4 Oe) down to -11.6 Oe (12.1 Oe) for 'up' ('down') magnetized configuration, in the case of H_C^{SL}, and from 52.6 Oe (50.4 Oe) down to 4.2 Oe (4.7 Oe) for 'up' ('down') magnetized configuration, in the case of H_C^{FL}, for a charge current density of $j = 10^6$ A cm^{-2} through the stripe. The strong decrease of both H_C^{SL} and H_C^{FL} stresses the importance of applying the PHE correction for a precise determination of the SOT induced fields when using the harmonic Hall voltage method.

Considering that the SHE in W layer is at the origin of the effective fields, we have calculated the effective spin Hall angle (θ_{SH}) using the relation [2, 30]: $H_C^{SL} = \hbar\theta_{SH}|j_W|/(2|e|M_S t_{CFA})$, where $\hbar$ is the reduced Planck's constant, e is the elementary charge, M_S is the saturation magnetization, j_W is the charge current density through the W layer and t_{CFA} is the thickness of the CFA layer. The charge current density flowing through the W layer was determined by considering a parallel resistor model, in which the current passes through both the W and the CFA layer. Thus, $j_W = j\left(1 + \frac{t_{CFA}}{t}\right)\frac{R}{R_W}$, where R is the measured stripe resistance and R_W is the calculated W layer resistance using the W resistivity determined from figure 1(b). Figure 6(a) shows the effective spin Hall angle for samples with different W thicknesses, which allowed us to determine the β-W bulk spin Hall angle $\theta_{SH}^{\infty} = 0.3 \pm 0.03$ and spin diffusion length $\lambda_{sf} = 2.2 \pm 0.3$ nm using the relation $\theta_{SH}^{\infty} = \theta_{SH}^{\infty}[1 - \mathrm{sech}(t/\lambda_{sf})]$ [31].

Moreover, in order to demonstrate the potential of this system for spin orbitronic devices with spin-torque driven magnetization manipulation, we have performed current-induced magnetization switching experiments. They have been carried out for the sample having a 5.5 nm thick W layer, using a pulsed dc current with a pulse width of 100 μs and a 2 ms interval between pulses. The switching was detected

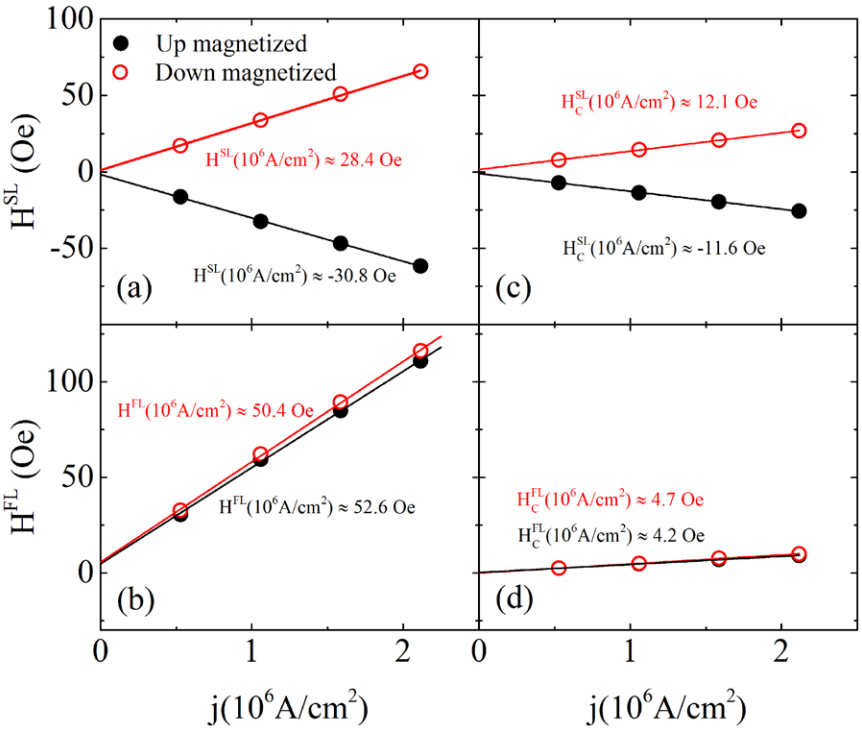

Figure 4. (a) and (b) Longitudinal (H^{SL}) and transverse (H^{FL}) SOT-induced effective fields, for the W(5.5 nm)/CFA(0.8 nm)/MgO(1.0 nm) sample, versus the charge current density, as determined using equation (1). (c) and (d) The effective fields versus the charge current density after the planar Hall effect correction. The values of the effective fields for the 'up' and 'down' magnetized configuration at a charge current density $j = 10^6$ A cm^{-2} are also given.

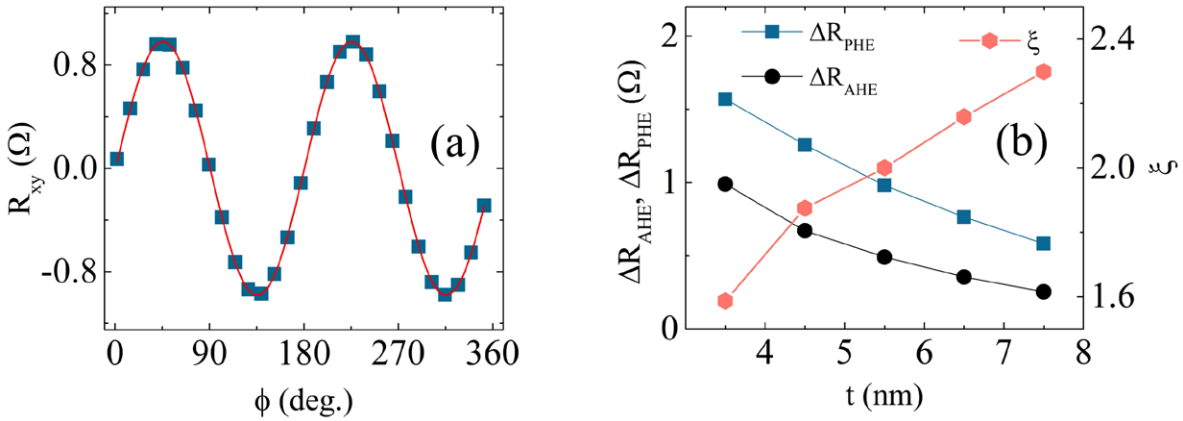

Figure 5. (a) Planar Hall measurements for the W(5.5 nm)/CFA(0.8 nm)/MgO(1.0 nm) structure. The red curve stands for a fit of the data using equation (3). (b) ΔR_{PHE}, ΔR_{AHE} and ξ ratio with respect to the W layer thickness.

by measuring the Hall voltage for each pulse. In order to ensure a deterministic switching of the magnetization a longitudinal bias field was applied. Figures 6(c) and (d) show typical switching cycles recorded for negative and positive longitudinal bias fields. The noise around zero current is a measurement artefact and it is due to the relatively low measured voltage due to the low current amplitude. The polarity of the switching loops is consistent with the negative value of the spin Hall angle of β-W. By reversing the direction of the bias field, the polarity of the switching loops reverses, which is in agreement with the SHE switching induced picture [2]. Furthermore, we have determined the switching current density for bias fields up to 250 Oe (figure 6 (b)). The switching current density was determined as an average between the positive and negative switching current densities. Each measurement cycle was repeated 10 times and the error bars correspond to the standard deviation from the mean value. The switching current density shows a rapid decrease with the bias field up to a field of about 50 Oe, above which the decrease shows a much lower rate. We experimentally observe that for bias fields above 50 Oe a sharp switching can be obtained for charge current densities of about 1.5×10^6 A cm^{-2}. The low switching current density observed in our samples is a consequence of several factors: the relatively large spin Hall angle of β-W, the relatively low damping and anisotropy field of the Heusler ferromagnet and the relatively large field like torque

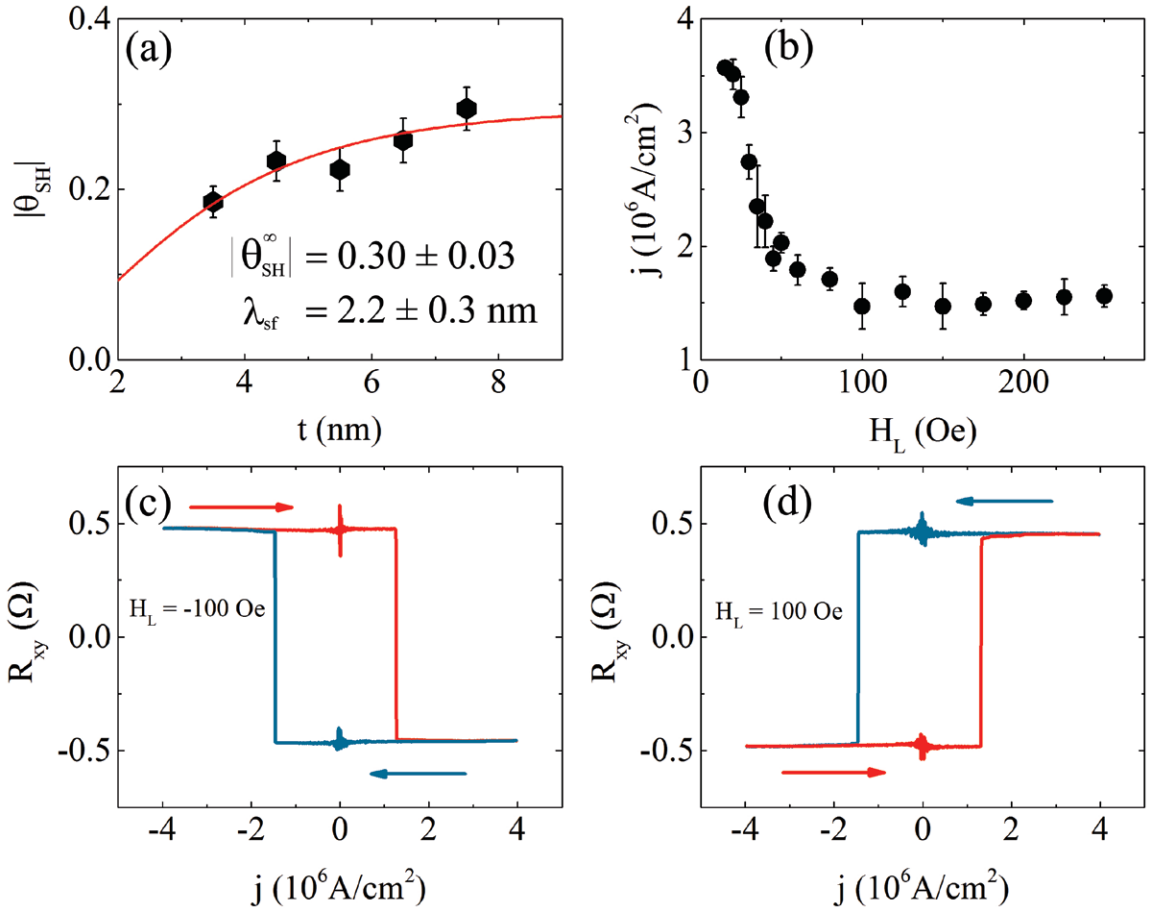

Figure 6. (a) Effective spin Hall angle versus the W layer thickness, the red line stands for theoretical fitting. The values of the bulk spin Hall angle and spin diffusion length are given. (b) Switching current density versus the longitudinal bias field for the W (5.5 nm)/CFA(0.8 nm)/MgO(1.0 nm) structure. (c) and (d) Typical current induced magnetization switching loops measured for negative and positive longitudinal bias fields.

[32, 33]. Moreover, it also has to be taken into account that the current induced switching is a complex process involving current induced nucleation in the presence of thermal effects, of the Dzyaloshinskii–Moriya interaction and of the field-like SOT [34, 35].

Conclusions

In summary, we have experimentally investigated the SOTs in β-W/Co_2FeAl/MgO structures showing PMA in the as-deposited state. We evaluated the Slonczewski-like and the field-like current induced effective fields using harmonic measurements. We highlight the essential role of the PHE corrections, which strongly alter the magnitudes of the effective fields. Using harmonic Hall measurements, we estimate for bulk β-W an effective spin Hall angle as large as 0.3 ± 0.03 and a spin diffusion length of 2.2 ± 0.3 nm. Moreover, we demonstrate SOT induced magnetization switching for current charge current densities of the order of 10^6 A cm^{-2}, which makes the β-W/Co_2FeAl/MgO system an interesting candidate for future spin–orbit torque spintronic devices.

Acknowledgments

This work was supported by UEFISCDI through PN-II-RU-TE-2014-1820—SPINCOD research grant No. 255/01.10.2015.

References

[1] Miron I M, Garello K, Gaudin G, Zermatten P-J, Costache M V, Auffret S, Bandiera S, Rodmacq B, Schuhl A and Gambardella P 2011 *Nature* **476** 189
[2] Liu L, Lee O J, Gudmundsen T J, Ralph D C and Buhrman R A 2012 *Phys. Rev. Lett.* **109** 096602
[3] Liu L, Pai C-F, Li Y, Tseng H W, Ralph D C and Buhrman R A 2012 *Science* **336** 555
[4] Avci C O, Garello K, Miron I M, Gaudin G, Auffret S, Boulle O and Gambardella P 2012 *Appl. Phys. Lett.* **100** 212404
[5] Moore T A, Miron I M, Gaudin G, Serret G, Auffret S, Rodmacq B, Schuhl A, Pizzini S, Vogel J and Bonfim M 2008 *Appl. Phys. Lett.* **93** 262504
[6] Miron I M *et al* 2011 *Nat. Mater.* **10** 419

[7] Haazen P P J, Murè E, Franken J H, Lavrijsen R, Swagten H J M and Koopmans B 2013 *Nat. Mater.* **12** 299
[8] Chiba D, Kawaguchi M, Fukami S, Ishiwata N, Shimamura K, Kobayashi K and Ono T 2012 *Nat. Commun.* **3** 888
[9] Emori S, Bauer U, Ahn S-M, Martinez E and Beach G S D 2013 *Nat. Mater.* **12** 611
[10] Ryu K-S, Thomas L, Yang S-H and Parkin S 2013 *Nat. Nano* **8** 527
[11] Liu L, Pai C-F, Ralph D C and Buhrman R A 2012 *Phys. Rev. Lett.* **109** 186602
[12] Liu R H, Lim W L and Urazhdin S 2013 *Phys. Rev. Lett.* **110** 147601
[13] Demidov V E, Urazhdin S, Ulrichs H, Tiberkevich V, Slavin A, Baither D, Schmitz G and Demokritov S O 2012 *Nat. Mater.* **11** 1028
[14] Pai C-F, Liu L, Li Y, Tseng H W, Ralph D C and Buhrman R A 2012 *Appl. Phys. Lett.* **101** 122404
[15] Miron I M, Gaudin G, Auffret S, Rodmacq B, Schuhl A, Pizzini S, Vogel J and Gambardella P 2010 *Nat. Mater.* **9** 230
[16] Wang X and Manchon A 2012 *Phys. Rev. Lett.* **108** 117201
[17] Kim K-W, Seo S-M, Ryu J, Lee K-J and Lee H-W 2012 *Phys. Rev.* B **85** 180404
[18] Wang W, Sukegawa H, Shan R, Mitani S and Inomata K 2009 *Appl. Phys. Lett.* **95** 182502
[19] Belmeguenai M, Tuzcuoglu H, Gabor M S, Petrisor T, Tiusan C, Berling D, Zighem F, Chauveau T, Chérif S M and Moch P 2013 *Phys. Rev.* B **87** 184431
[20] Kim J, Sinha J, Hayashi M, Yamanouchi M, Fukami S, Suzuki T, Mitani S and Ohno H 2013 *Nat. Mater.* **12** 240
[21] Hayashi M, Kim J, Yamanouchi M and Ohno H 2014 *Phys. Rev.* B **89** 144425
[22] Garello K, Miron I M, Avci C O, Freimuth F, Mokrousov Y, Blugel S, Auffret S, Boulle O, Gaudin G and Gambardella P 2013 *Nat. Nano* **8** 587
[23] Lee H-R, Lee K, Cho J, Choi Y-H, You C-Y, Jung M-H, Bonell F, Shiota Y, Miwa S, and Suzuki Y 2014 *Sci. Rep.* **4** 6548
[24] Chen Y-T, Takahashi S, Nakayama H, Althammer M, Goennenwein S T B, Saitoh E and Bauer G E W 2013 *Phys. Rev.* B **87** 144411
[25] Nakayama H, Althammer M, Chen Y T, Uchida K, Kajiwara Y, Kikuchi D, Ohtani T, Geprägs S, Opel M, Takahashi S, Gross R, Bauer G E W, Goennenwein S T B and Saitoh E 2013 *Phys. Rev. Lett.* **110** 206601
[26] Althammer M *et al* 2013 *Phys. Rev.* B **87** 224401
[27] Cho S and Park B-G 2015 *Curr. Appl. Phys.* **15** 902
[28] Cho S, Chris Baek S-h, Lee K-D, Jo Y and Park B-G 2015 *Sci. Rep.* **5** 14668
[29] Kim J, Sheng P, Takahashi S, Mitani S and Hayashi M 2016 *Phys. Rev. Lett.* **116** 097201
[30] Khvalkovskiy A V, Cros V, Apalkov D, Nikitin V, Krounbi M, Zvezdin K A, Anane A, Grollier J and Fert A 2013 *Phys. Rev.* B **87** 020402
[31] Liu L, Moriyama T, Ralph D C and Buhrman R A 2011 *Phys. Rev. Lett.* **106** 036601
[32] Lee K-S, Lee S-W, Min B-C and Lee K-J 2013 *Appl. Phys. Lett.* **102** 112410
[33] Taniguchi T, Mitani S and Hayashi M 2015 *Phys. Rev.* B **92** 024428
[34] Perez N, Martinez E, Torres L, Woo S-H, Emori S and Beach G S D 2014 *Appl. Phys. Lett.* **104** 092403
[35] Lee O J, Liu L Q, Pai C F, Li Y, Tseng H W, Gowtham P G, Park J P, Ralph D C and Buhrman R A 2014 *Phys. Rev.* B **89** 024418